Yielding of a Model Glassy Polycarbonate under Tension: A Molecular Mechanics Simulation

Cun Feng Fan†

Pasadena Advanced Research Center, Molecular Simulations Inc., 600 South Lake Avenue, Suite 411, Pasadena, California 91101

Received September 20, 1994; Revised Manuscript Received May 5, 1995®

ABSTRACT: Yielding of a model glassy polycarbonate under tension was studied using the molecular mechanics method. The model structures were stretched by changing the cell dimensions consistent with the applied strain and the assumed Poisson ratio. After the deformation, the model structures were optimized. The resultant stress–strain curves clearly indicate the yielding of the model polymer near 13% strain. The nonbonded van der Waals interactions represent the dominant contribution to the overall strain energy. The yield stress and yield strain obtained from the simulation compare favorably with the experimental data if the latter are extrapolated to 0 K. To further examine the yielding phenomenon, the same deformation scheme and an affine model were applied to a model atomic glass. The results support the idea that the nature of yielding is the inflection exhibited on the Lennard-Jones potential representing the van der Waals interactions. The structural changes of the model polymer were studied through analyses of the Voronoi volume distribution of atoms, the segmental orientation, and the overall chain deformation and orientation. Voids were developed during the deformation.

Introduction

Yielding of an amorphous polymer under shear deformation has been observed in recent molecular mechanics studies of polypropylene and polycarbonate.[1–3] It was also seen in a molecular dynamics study of a model polyethylene under tension.[4] These studies clearly demonstrate that the atomistic simulation is capable of reproducing some important mechanical properties of amorphous polymeric materials, even under very large deformations. Since the models are constructed on the atomistic level, detailed structure changes upon yielding can be investigated. Additional discussions were also presented in these studies. Because of the ample information generated from simulation, one would expect to gain more insight about the fundamental factors governing the yielding phenomenon. Yielding is normally defined as the point on the stress–strain curve where the stress exhibits the maximum value. More precisely, it is the point where the first derivative of strain energy with respect to strain, which is the stress, shows a maximum or the second derivative (the modulus) becomes zero. Therefore, it is the inflection point on the strain energy versus strain plot. In our previous study of tensile deformation of a model polycarbonate, it was found that the nonbonded van der Waals interaction contributes the most to the overall strain energy.[5,6] The strain energy versus strain curve largely resembles in shape that of the Lennard-Jones potential. Based on these observations, it was concluded that the nature of yielding is due to the characteristics of the Lennard-Jones potential (or other similar potentials) when the van der Waals interactions are the dominant interactions.

The Lennard-Jones pair potential can be expressed as

$$U = D_0(\varrho^{-12} - 2\varrho^{-6}) \tag{1a}$$

where $\varrho = r/r_0$. The D_0 and r_0 are constants and r is the distance between two atoms. The first and second derivatives of $U(\varrho)$ are

$$\frac{dU}{d\varrho} = -12D_0(\varrho^{-13} - \varrho^{-7}) \tag{1b}$$

$$\frac{d^2U}{d\varrho^2} = 12D_0(13\varrho^{-14} - 7\varrho^{-8}) \tag{1c}$$

Figure 1 shows the plots of $U-\varrho$, an analog of the strain energy–strain curve, and $dU/d\varrho-\varrho$, similar to the stress–strain curve. The inflection on $U-\varrho$ or the maximum on $dU/d\varrho-\varrho$ is given by

$$\varrho = \left(\frac{13}{7}\right)^{1/6} = 1.1087 \tag{1d}$$

Therefore, the nature of yielding for a material dominated by the van der Waals interactions is due to the increase of distance between atoms when they pass through the inflection point on the $U-\varrho$ plot. Quantitatively, the Lennard-Jones potential will lead a material to yield near 10.87% strain, and it is universal as long as the van der Waals interaction is dominant.

This conclusion removes any magic veil covering the nature of yielding. Experimental data support such a conclusion, since most polymers yield at about 5–10% strain.[7] However, this is still an oversimplification. In a polymer system, energy change between any pair of atoms may be described by eq 1a only if (1) the two atoms have an initial distance of r_0, (2) the vector pointing from one atom to the other coincides with the draw direction, and (3) their displacement is not affected by the connectivity. For all the pairs contributing to the strain energy, only a few might meet these conditions if there are any at all. The majority will have a different relationship between pair energy and applied strain than the one shown in Figure 1.

In this paper, we examine the yielding phenomenon in detail. We report an in depth molecular mechanics study of tensile deformation of a model polycarbonate glass and an atomic amorphous glass. The latter example is used since we are able to use an affine model to describe the atomic position changes during deformation. Therefore, we can predict the energy–strain curve

† Mailing address: Beckman Institute (139-74), California Institute of Technology, Pasadena, CA 91125.

® Abstract published in *Advance ACS Abstracts,* June 15, 1995.

0024-9297/95/2228-5215$09.00/0

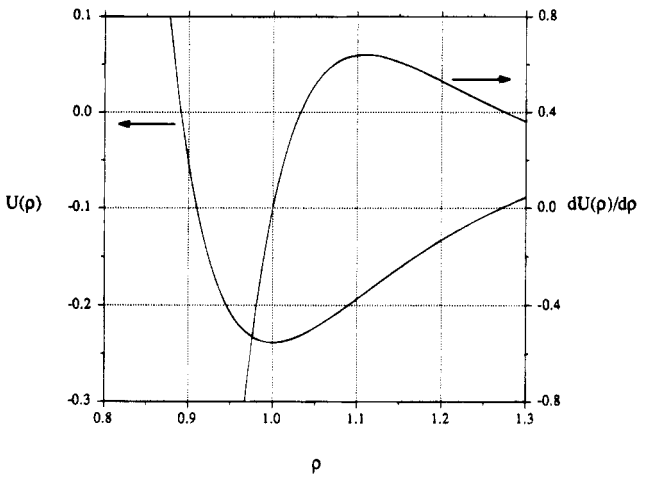

Figure 1. Lennard-Jones potential and its first derivative.

Table 1. Averaged Cell Parameters of the Microstructures

	atomic glass	polycarbonate
a (Å)	31.07 ± 1.42	19.75 ± 0.39
b (Å)	30.84 ± 2.04	19.73 ± 0.28
c (Å)	30.48 ± 1.91	19.71 ± 0.51
α (deg)	88.38 ± 4.27	91.43 ± 1.92
β (deg)	89.74 ± 0.57	90.63 ± 0.89
γ (deg)	89.68 ± 1.75	90.36 ± 1.62
d (cm^3/g)	1.67 ± 0.03	1.15 ± 0.06

for every pair. The sum of these curves will be compared with the one generated from simulation where the atomic positions are determined by the structural optimization. This comparison will reveal if the Lennard-Jones potential is responsible for the yielding. The atomic model is needed since the use of the affine model to calculate the energy change of covalently connected atoms in the polymer will be unrealistic and erroneous. We present a representative stress–strain curve for a model polycarbonate. The structural changes, such as the changes in volume, overall chain conformation, segmental orientation, and the void generation, are analyzed. Some views regarding the shear and compressive yielding are also presented.

Models and Simulation

A. Models. The full atomic model of amorphous Bisphenol A polycarbonate contains 691 atoms (DP = 21). Model structures were prepared through several cycles of energy minimization and molecular dynamics. In the final stage, a full optimization of cell parameters and coordinates was performed. Six sample structures were constructed. All of them are triclinic. The averaged cell parameters are listed in Table 1. The details of the model construction, structure, and mechanical properties at small strain were described in an earlier paper.[6] A modified version of the the Dreiding force field is used to represent the interactions between atoms.[6,8]

Six configurations of a model atomic amorphous glass with 729 argon atoms were extracted from a 100 ps *NVT* molecular dynamics trajectory at 90 K. The final samples were obtained from full structural optimization of these configurations. The average cell parameters of these structures are also listed in Table 1. The force field parameters D_0 and r_0 for eq 1a were 3.8164 Å and 0.2384 kcal/mol, respectively.[9]

B. Simulation. 1. Tensile Deformation through Molecular Mechanics. There are several methods to obtain a stress–strain curve using molecular mechanics simulation. Here, we use a stress–strain curve in the z direction, i.e., σ_{33}–ϵ_{33}, as an example. In the *zyx* convention, the **c** lattice vector coincides with the z axis of the Cartesian frame and **b** is in the yz plane. The first method is to apply an external stress, σ_{33}, incrementally and optimize the cell parameters and coordinates at each stress value. The strain component, ϵ_{33}, is obtained from the change in the c axis. In the second method, a strain is imposed by fixing the c axis at a value corresponding to this strain, and the other cell parameters as well as the coordinates are optimized. The stress, σ_{33}, is obtained from the corresponding component of the internal stress tensor. These two methods are analogs to the real tensile stretching experiment and either one would be a natural choice in the simulation. However, there are some shortcomings in the simulation. In the first method, when the maximum stress is approached (near yielding), the c axis will keep increasing and the cell optimization will never converge. The second method requires a constraint cell optimization to be used (fixed length in c) which converges very slowly, especially at large strain values, if it converges at all. We did use this method in an earlier study; however, the convergence criteria for cell optimization was reduced greatly.

In this study, we tried to avoid these problems caused by cell optimization and still simulate the deformation process as realistically as possible. We applied a strain, ϵ_{33}, by changing the c axis and simultaneously changing other cell parameters in accord with an assumed Poisson ratio for the model. Hence, only the coordinates are optimized under the new set of cell parameters. As in the second method, the stress σ_{33} is obtained from the internal stress tensor after the minimization. One additional convenience of this method is that the deformation pattern is known prior to the minimization, and this allows us to use an affine model as a reference in the energy calculation and/or structure analysis. It is important in this method that the Poisson ratio represents the intrinsic mechanical properties of the model. In the first two methods, the Poisson ratio emerges naturally from the cell optimization.

2. Poisson Ratio of a Material. The Poisson ratio is defined as the negative of the ratio of the strain in the perpendicular direction to the strain in the draw direction at infinitesimal strain

$$\nu = \lim_{\epsilon_L \to 0}\left(-\frac{\epsilon_r}{\epsilon_L}\right) \tag{2}$$

where ϵ_L is the strain in the draw direction and ϵ_r the is strain in the direction perpendicular to the draw direction. If $\nu = 0.5$ the volume will remain constant during deformation. For $\nu < 0.5$, the volume will increase upon stretching and decrease upon compression, and the opposite is true if $\nu > 0.5$. At a finite strain, an apparent Poisson ratio can be defined as

$$\nu_a = -\frac{\epsilon_r}{\epsilon_L} \tag{3}$$

If ν is an intrinsic property of the material and remains constant during deformation (this may not be true for a real material), then ν_a will change as a function of strain. The relationship between ν_a, ν, and

ϵ_L is (see Appendix A)

$$\nu_a = \frac{1 - (2\epsilon_L + 1)^{-\nu}}{2\epsilon_L} \tag{4}$$

In the simulation, we assigned ν of 0.27 for both the polycarbonate and the atomic glass. This intermediate value is chosen using the result of the stiffness matrix calculation (0.24) and the larger deformation (0.31) of a model polycarbonate from an earlier study.[6] This value is also close to the one obtained from the stiffness matrix of the model atomic glass (0.25).

3. Deformation process. For each model structure, three stress–strain curves are recorded representing measurements in three independent directions. The applied strain tensors for these three cases are

$$\epsilon = \begin{pmatrix} \epsilon & 0 & 0 \\ 0 & -\epsilon\nu_a & 0 \\ 0 & 0 & -\epsilon\nu_a \end{pmatrix} \tag{5a}$$

$$\epsilon = \begin{pmatrix} -\epsilon\nu_a & 0 & 0 \\ 0 & \epsilon & 0 \\ 0 & 0 & -\epsilon\nu_a \end{pmatrix} \tag{5b}$$

$$\epsilon = \begin{pmatrix} -\epsilon\nu_a & 0 & 0 \\ 0 & -\epsilon\nu_a & 0 \\ 0 & 0 & \epsilon \end{pmatrix} \tag{5c}$$

and the measured stress components are σ_{11}, σ_{22}, and σ_{33}, respectively. Hence a total of 18 stress–strain curves were generated for both the polycarbonate and the atomic glass (three curves for each sample with six samples).

One of the key steps in the simulation is to obtain the new set of cell parameters corresponding to the applied strain. The exact procedure for such calculation for any shape of unit cell was described in the earlier paper.[6] Each stress–strain curve was generated with a strain increment of 0.002. The maximum strain is 0.3 (30%). The new set of cell parameters corresponding to the applied strain tensor was calculated from the original shape matrix and the definition of the strain tensor.[6,9,10] For each set of cell parameters, only the atomic positions were optimized. The energy and stress changes of the system as a function of strain were then recorded. The resulting structures were saved for further analysis.

4. Affine Deformation Model. The affine deformation model was also used to calculate the energy changes in the atomic glass. Affine deformation assumes that the components of each vector in the system transform linearly with the macroscopic deformation, i.e., the applied strain.[12] If one uses the cell vectors as basis vectors to express the atomic positions, the components of these position vectors will not change under an affine deformation. The scaled components of a vector ($\mathbf{x}_s$) are related to its Cartesian components ($\mathbf{x}$) through the shape matrix $\mathbf{h}$

$$\mathbf{x}_s = \mathbf{h}^{-1}\mathbf{x} \tag{6a}$$

$$\mathbf{x} = \mathbf{h}\mathbf{x}_s \tag{6b}$$

The $\mathbf{x}_s$ was calculated from $\mathbf{h}_0^{-1}$, the inverse of the shape and size matrix of the undeformed cell. These do not change throughout the affine deformation. At each strain value, the new set of cell parameters and corresponding $\mathbf{h}$ matrix were obtained. The new Cartesian components of each vector, $\mathbf{x}$, are then obtained through eq 6b.

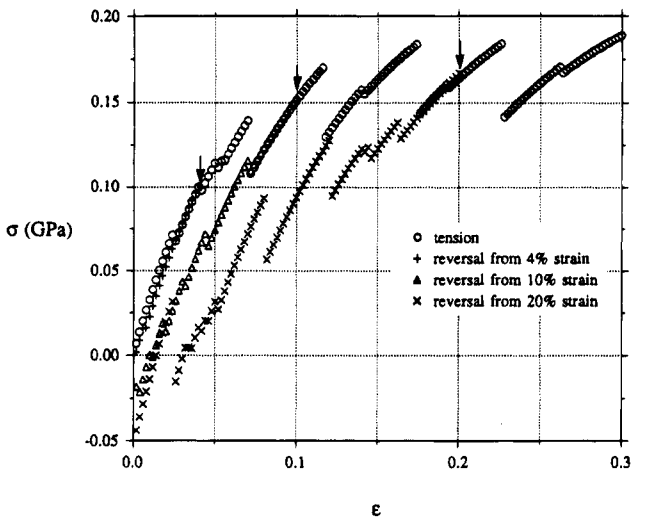

Figure 2. A single stress–strain curve of the model atomic glass (open circles). The arrows indicate the beginning of the reversal deformation. The reversal stress–strain curves start from 4% (+), 10% (Δ), and 20% (×) strain.

In the calculation of the strain energy of the atomic glass, the $\mathbf{x}_s$ was the scaled components of the pair distance vector ($\mathbf{r}_{ij}$). Its Cartesian components were determined at each strain value (from the corresponding $\mathbf{h}$ matrix). Equation 1a was then used to calculate $U(\varrho)$. Summation over all the pairs (using minimum image convention) produces the strain energy–strain curves. The first derivative (obtained by the finite difference method) of this curve yields the stress–strain curve of the affine deformation model. If the distance between two atoms becomes less than $0.89r_0$ ($\sigma = 0.89r_0$), the $U(\varrho)$ of the pair is assigned to be zero (see Figure 1) to exclude the overlap between atoms. This treatment may be interpreted as follows: if the two atoms overlap, the repulsive force immediately takes effect and pushes these atoms back to a distance of $r = \sigma$.

Results and Discussion

A. Stress–Strain Curves and Nature of Yielding. 1. Stress–Strain Curve of Model Atomic Glass. Figure 2 shows a typical stress–strain curve of the model atomic glass. Stress initially increases linearly with the strain and then shows a discontinuity, forming several parallel short curves. The discontinuity in the stress–strain plot is caused by the discontinuity in the strain energy as a function of strain, indicating that at those positions the system may move from one local minimum to another. Due to the large dimension and the complexity of the potential energy surface, it might have a considerable number of low-energy barriers between local minima. External force (the applied strain in this case) helps the atoms to change their positions and moves the system away from one minimum to another. The reversibility of the tensile deformation is studied by compressing the system at three strain positions: 4, 10, and 20%, respectively, as indicated by the arrows in Figure 2. The compression curves essentially follow the continuous part of the tension curve. At those jump positions, the compression curves tend to follow their own trend instead of jumping back to the tensile curves. The compression curves themselves also exhibit jumps similar to those seen in

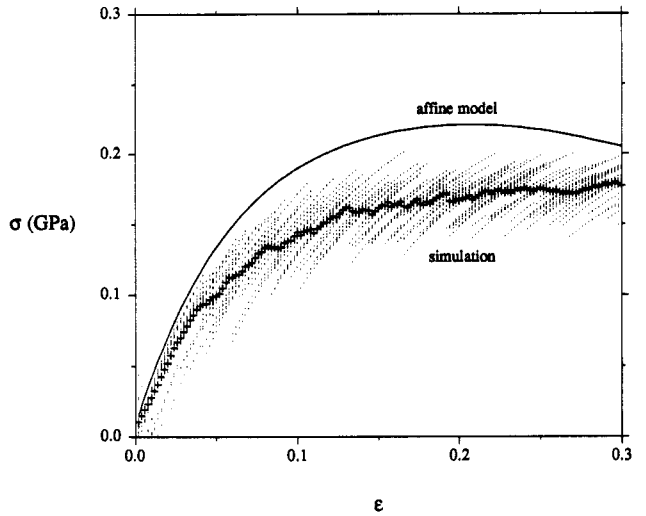

Figure 3. Stress–strain curves of the model atomic glass. The dots represent the original data. The crosses are the averaged data, and the solid line is obtained from an affine model.

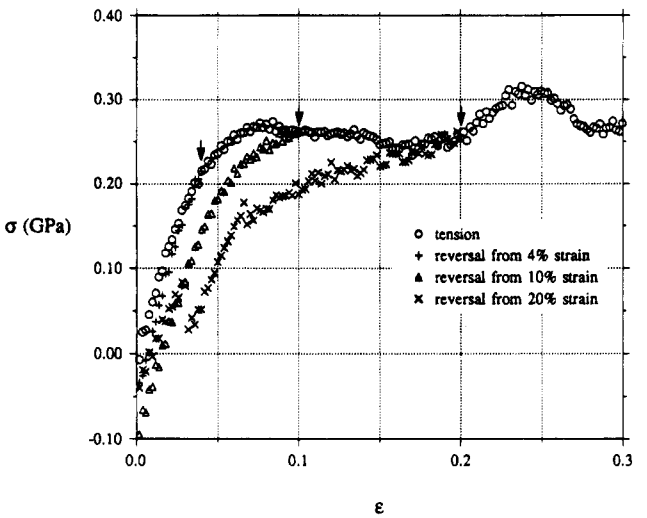

Figure 4. A single stress–strain curve of the model polycarbonate (open circles). The arrows indicate the beginning of the reversal deformation. The reversal stress–strain curves start from 4% (+), 10% (Δ), and 20% (×) strain.

tension, due to the same reason. The overall shape of the curve shows that yielding occurs above 10% strain.

The stress–strain curve shown in Figure 2 represents the typical deformation behavior of an individual model microstructure. Certain features shown here may be general, such as the yielding, and others are more or less accidental, such as the positions of the discontinuities. Figure 3 shows the averaged stress–strain curves of the atomic glass, along with the original data. The original 18 stress–strain curves are similar to the one shown in Figure 2 and plotted here as background to demonstrate the range of stress variation at each strain. The calculated result from the affine deformation model is also plotted for comparison. The averaged stress–strain curves reveal a common feature in all of the individual microstructures. Yielding occurs around 12% strain. The precise position may not be determined easily nor is it critically important.

The simple affine deformation model reproduces the basic feature of the stress–strain from simulation. The model is merely the sum of the Lennard-Jones interactions from all the pairs in the system with a consideration of their initial orientations and distances. It is clear that the characteristics of the Lennard-Jones potential, i.e., the inflection at $\varrho = 1.1087$, causes the material to yield around 10% strain. There is a certain discrepancy between the affine model and simulation as the stresses from the affine model are higher than those of the simulation. Affine deformation only provides a very rough description of the deformation process. The optimal atomic positions upon deformation may be around those calculated from the affine model, however, only energy minimization can determine where they are.

2. Stress–Strain Curve of Model Polycarbonate. Figure 4 shows the stress–strain curve of the model polycarbonate. It is essentially continuous, indicating that jumping from one local minimum to another is not as easy as in the atomic glass. The model shows yielding occurs at about 8% strain. Reversible deformation occurs only at small strain (~4%). At larger strain values, beyond yielding the compression curves soon depart from the corresponding tension curves. It is interesting to note that the compression curve always falls below the initial tension curve. A similar phenomenon, hysteresis, is commonly observed in experiments. The energy loss (the area under the stress–strain curve is the strain energy) normally is in the form of heat, which increases the temperature of the specimen. In molecular mechanics, the irreversible behavior (the hysteresis) stems mostly from the flattening of the overall potential energy surface after the inflection (the yielding) and having nearby and accessible multiple solutions to the energy–microstate function. In the deformation of increasing energy, the change of microstructure follows the path requiring the minimum structural change (the extreme is affine deformation). In the reversal process, the change of microstructure may choose a path with a smaller energy gradient from a large number of available lower energy states. Another interesting phenomenon shown on the reversal stress–strain curves is the slight shift of the stress-free state toward larger dimension. At the zero strain (the original stress-free state) the stress becomes negative (compressive stress). The stress-free state can only be reached if the sample retains a small amount of tensile strain.

Similar to the model atomic glass, one expects the yielding shown on the stress–strain curve in Figure 4 to be a general feature of the model polymer whereas the positions and the height of those hills and valleys on the curve to appear randomly. The rough stress–strain curve is not representative of the experimental stress–strain curve of polycarbonate, which is known as a smooth one. When the simulation cell is much smaller compared to the experimental scale, it is inevitable that a certain inhomogeneity and anisotropy will be introduced into the system. The smaller the model, the more severe the problem is. More representative characteristics of the material can be derived only when an ensemble of small microstructures is used to average out those features due to the "noise". Figure 5 shows the averaged stress–strain curve of the polycarbonate as well as the original data. Apparently the data become more scattered as the strain increases. A well defined yield point occurs near 14% strain on the averaged stress–strain curve. The lower and higher edges of the envelope of the original data form smooth curves. The lower one represents the microstructures in the ensemble with the lowest stress for a given strain. Therefore, the curve itself is representative of the stress–strain curve of the system under a more ideal

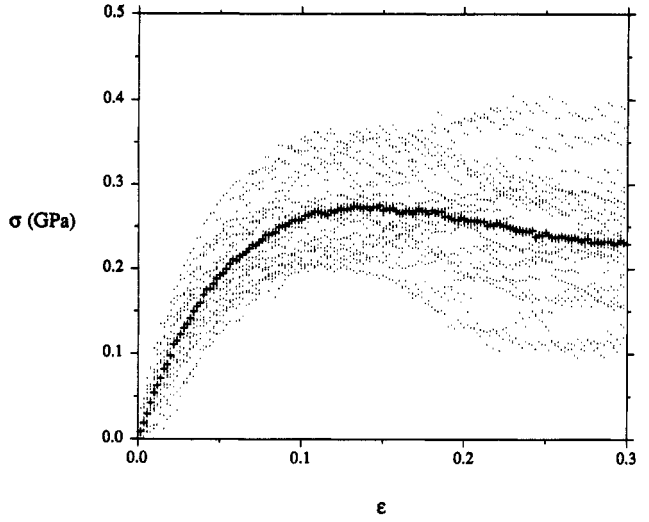

Figure 5. Stress–strain curves of the model polycarbonate. The dots represent the original data, and the crosses are the averaged data.

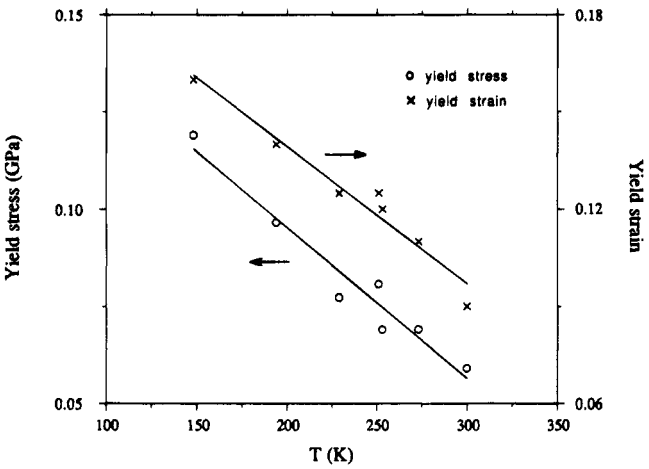

Figure 6. Experimental data of yield stress and yield strain as a function of temperature (data from ref 14).

circumstance; i.e., the system has a chance to find a low energy and stress state.

3. Comparison with Experimental Data. The mechanical properties of polycarbonates have been studied extensively.[13] Several stress–strain curves measured under various conditions were given in ref 14. One of the relevant experiments was on the measurements of the stress–strain curves of poly(Bisphenol A carbonate) at different temperatures.[15] Figure 6 shows the yield stress and the yield strain as a function of temperature. The data were taken from the original stress–strain curves given in ref 14. From 148 to 300 K, the yield strain decreases from 16% to about 8% while the yield stress reduces from 0.119 to 0.059 GPa. Similar trends have been observed in other polymers as well.[16] The simulation gives a yield strain of about 14% and a yield stress of 0.27 GPa if the averaged stress–strain curve is used. The yield strain and stress from the lower limit of the original data are about 12% and 0.20 GPa, respectively. For a more reasonable comparison, the relationship between the molecular mechanics simulation and the temperature should also be considered.

Unlike the molecular dynamics simulation, the energy minimization assumes no thermal motion; therefore it simulates the behavior of a material near 0 K. At such low temperatures, any real polymer becomes brittle and

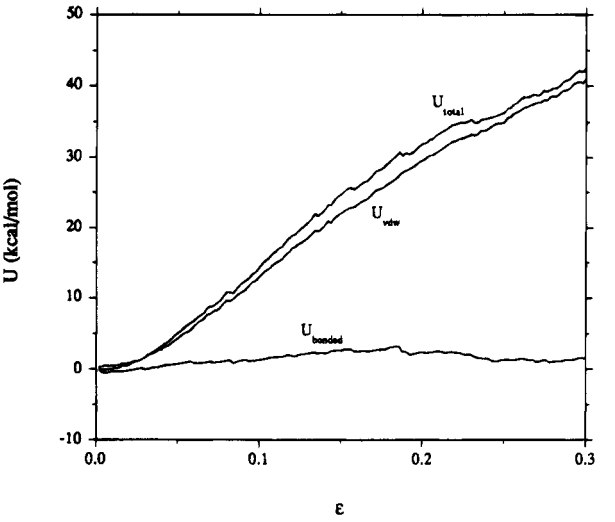

Figure 7. Total strain energy and its components of the model polycarbonate as a function of strain.

no yielding would be seen. In the above experiments, the data at 116 K show no sign of yielding, and the sample fails at 10% strain with a stress of 0.124 GPa.[14,15] Then, how valid is the conclusion drawn from the simulation and how can it be related to the experimental data? To answer this question, one may assume that at a certain finite temperature (below the glassy transition) the thermal motion of the atoms will lead them to fluctuate near a set of positions corresponding to the applied strain. This set of positions will change with the applied strain. At very low temperatures, atoms lose mobility; thus they will not be able to move to the new set of positions corresponding to the applied strain nor will they fluctuate around them. Hence the material becomes brittle. However, the energy minimization represents a different situation; it can move atoms to the new set of positions corresponding to the applied strain and then freeze them, still excluding the thermal fluctuation. This is an artificial process realized only in the molecular mechanics simulation. However, the conclusions drawn from the energy minimization should similarly be valid as they were from the molecular dynamics in which the interactions are determined mainly by the average positions. The molecular mechanics simulation reveals no temperature dependent information. Therefore, the molecular mechanics simulation is capable of locating the yield point if a material yields under tension. However, it will not tell at what temperature it will yield.

The comparison of molecular mechanics simulation results with experiments should be made by extrapolating the experimental data to 0 K somehow. Here, we use a simple linear extrapolation. Such extrapolation may not always be valid, especially when certain structural transition occurs. If we extrapolate the experimental data in Figure 6, the yield strain and the yield stress are 0.22 and 0.17 GPa, respectively. The simulated yield stress is only 14% higher than the experimental data if we use the lower limit curve. The difference between the yield strains seems larger, however, the yielding peak itself is very broad (about 10% strain range). Therefore, we consider that the simulation results compare favorably with the experimental data.

4. Nature of Yielding. Figure 7 plots the strain energy of polycarbonate as a function of strain. The contributions from covalent energy terms (the sum of

energies from bonds, angles, torsions, and inversions) are small since the higher force constants of these covalent terms will relax first upon minimization and retain the geometry near undeformed values. Thus, the dominant contribution from the van der Waals interactions leads to the model polymer yielding near 13% strain, similar to the atomic glass. Combining the results obtained from both molecular mechanics simulations (atomic glass and polycarbonate) and the affine model calculation, it is clear that the nature of yielding for the model polymer is due to the inflection exhibited on the Lennard-Jones potential (or any similar potential) representing the van der Waals interactions. There are no other requirements for the yielding to occur rather than simply changing the distances between atoms to pass the inflection point. If there are any yielding related specific structural changes, being observed in either experiment or simulation, then these changes only facilitate the further movements of atoms with strain. They do not cause the yielding. Yielding can occur with or without any specific structural changes. This conclusion should be applicable to any material for which the interactions are dominated by van der Waals energy terms.

Materials may not yield near 11% strain if interactions other than van der Waals contribute the most to the strain energy. The inflection for the typical hydrogen-bonding interaction[8]

$$U_{hb} = D_{hb}\left[5\left(\frac{R_{hb}}{R_{DA}}\right)^{12} - 6\left(\frac{R_{hb}}{R_{DA}}\right)^{10}\right]\cos^4(\theta_{DHA}) \quad (7)$$

is at $R_{hb}/R_{DA} = 1.087$, if the hydrogen atom, the donor atom, and the acceptor atom are well aligned, i.e., $\theta_{DHA} = \pi$ or $\cos\theta_{DHA} = -1$. Here R_{DA} is the distance between the donor and acceptor atoms. D_{hb} and R_{hb} are force field parameters. No inflection point exists for the electrostatic potential[8]

$$U_Q = \frac{332.0637Q_iQ_j}{\epsilon R_{ij}} \quad (8)$$

Yielding behavior of the systems dominated by these types of interactions need to be studied separately. Well-oriented crystalline polymers will not yield near 11% strain, since the covalent terms, especially angle bending, will contribute the most to the strain energy.

Our preliminary study of the same models under simple shear and compressive deformation showed results similar to those observed in this work. Yielding occurred in both cases. The volume of the simulation cell does not increase in the simple shear deformation. The local rearrangements upon deformation will cause certain atoms to be separated. It is the inflection of these pair energies that contributes the most to the yielding. In the case of compression, the increase of distances between atoms mainly comes from the lateral expansion during deformation. In all three types of deformation (tension, compression, and shear) the distances between atoms can either increase or decrease, causing the pair energy to vary. It is the inflection on the total energy–strain curve that determines when yielding should occur. The fundamental source of this inflection was the inflection exhibited on the potentials representing the van der Waals interactions.

B. Structural Changes upon Deformation. The above section shows that it is the nature of the van der Waals interactions that leads a material to yield, and no specific structural changes are required for it to happen. However, it is very informative to characterize how the structures reorganize themselves during the deformation, especially at postyielding, since useful information related to failure may emerge from structural analysis. The following analysis mainly applies to the model polycarbonate, except the first section. The plots shown in the following sections are the average of 18 deformation processes (6 models and 3 draw directions for each model).

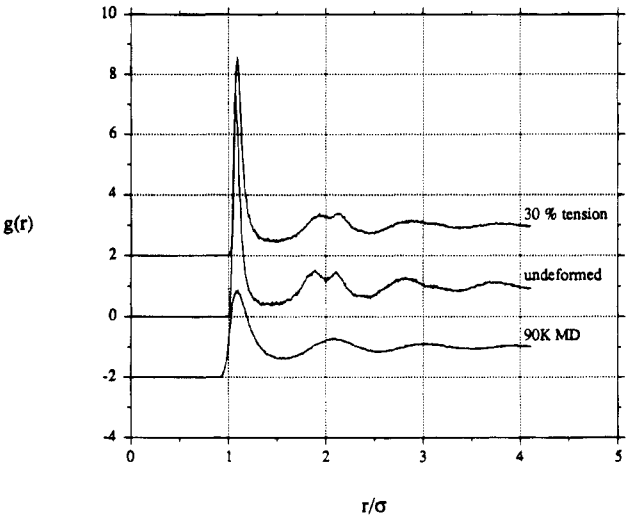

Figure 8. Radial distribution functions of the model atomic glass obtained from 90 K molecular dynamics (bottom), undeformed structures (middle), and after 30% strain (top). The vertical axis is shifted 2 units down for 90 K MD data and 2 units up for 30% strain data. The σ in units of the horizontal axis equals $0.89r_0$.

1. Packing and Volume Distributions. Figure 8 shows the pair distribution functions of the atomic glass before and after deformation as well as the one obtained from 90 K molecular dynamics. MD at 90 K generated a typical liquid structure. Structures after minimization are not a completely frozen liquid. The split of the second peak in Figure 8 clearly indicates the existence of partial order of a glassy structure. After 30% deformation, one sees the shifting and the broadening of all the peaks. Quantitatively, the peak position of the first shell shifted from 1.080 before deformation to 1.105 (r/σ) after 30% strain, which is a 2.3% change. However, the overall volume change of the system is 10.43% at 30% strain. An affine deformation would shift the peak position one third of 10.43%, i.e., 3.48%. The observation of a smaller (2.3%) shift in the simulation indicates that the atoms tend to pack closer than the uniform scaling.

The actual volume distribution on the atomic level was also analyzed using Voronoi volume distribution. The calculation was based on Appendix F.35 of ref 17. Slight modification was made to apply it to the triclinic unit cell, and the position of the faces separating neighboring polyhedrons was determined by the ratio of the van der Waals radii of the neighboring atoms. Figure 9 is the Voronoi volume distribution of the atomic glass. After 30% tensile strain, the peak position shift is about 11.4%, close to the overall volume change. It is not surprising that the summation of the Voronoi volumes of the system should equal the total volume of the system. The broadening of the peak indicates that the change of the atomic volume is uneven. The volumes of atoms with small volume (may be in the center of the clusters) increase less than those with

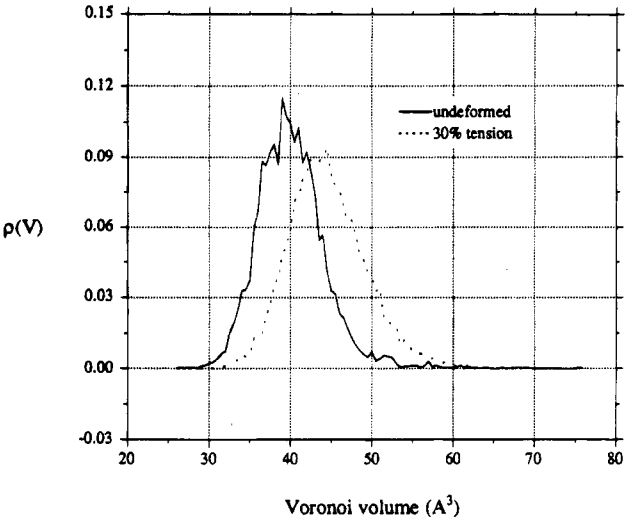

Figure 9. Voronoi volume distributions of the model atomic glass. The solid line represents undeformed structures, and the dotted line is for the structures after 30% strain.

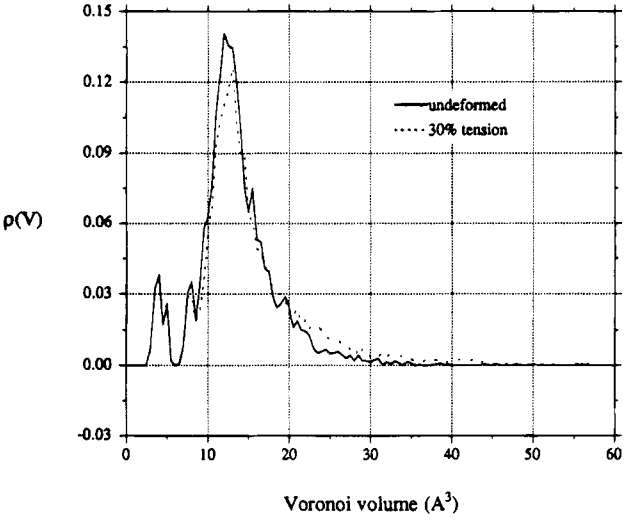

Figure 10. Voronoi volume distributions of the model polycarbonate. The solid line represents undeformed structures, and the dotted line is for the structures after 30% strain.

larger volumes. This observation matches the observation of a smaller shift for the first peak in the pair distribution function.

The Voronoi volume change of the model polycarbonate is very different (Figure 10). The covalently bonded atoms in the polymer will try to maintain their stable segmental structures against the force to separate them. For example, sp^3 carbon atoms (the peaks at <5 Å^3) bonded to four other atoms will always occupy the very same volume no matter what the total volume is. The same is true for the sp^2 carbon atoms of the phenyl ring. These atoms make up the majority of the system. This is the main reason that the curves in Figure 10 change very little as a function of strain. Those atoms at the "edge" of a segment naturally occupy more space when the volume of the system increases, since they do not suffer from the above-stated constraints. Some of those atoms changed their volume by 300%. However, since they spread over a broad volume range, the population at each of these larger volumes is small. Therefore, only a small increase in $\varrho(V)$ is seen at the larger volumes (>20 Å^3).

2. Segmental Orientation. A repeat unit of the polycarbonate is shown in Figure 11, where two vectors

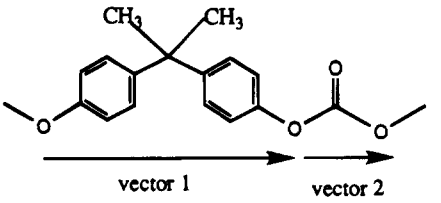

Figure 11. Schematic drawing of a repeat unit of polycarbonate. Vector 1 and vector 2 are defined to represent the orientation of the Bisphenol moiety and the carbonate moiety, respectively.

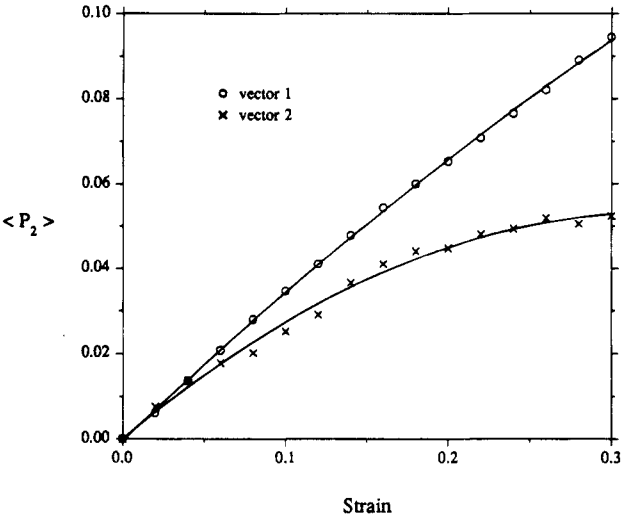

Figure 12. Segmental orientation functions (P_2) of the model polycarbonate as a function of strain. Vectors 1 and 2 are defined in Figure 11.

are defined. Vector 1 represents the Bisphenol moiety, while vector 2 represents the carbonate group. The orientation of these two groups can be characterized by the Hermans orientation function ($\langle P_2 \rangle$) of these two vectors[18]

$$\langle P_2 \rangle = \frac{1}{2}(3\langle \cos^2 \theta \rangle - 1) \qquad (9)$$

where θ is the angle between a vector and the draw direction. The average is over all vectors of the same type. A fully extended chain will have perfect orientation only if all bond angles along the backbone are the same. The variation of $\langle P_2 \rangle$ as a function of strain is plotted in Figure 12. The zero value of the $\langle P_2 \rangle$ values before deformation indicates a complete random orientation of the initial structure. Such randomness is achieved because all three Cartesian axes were independently chosen as the draw direction. Thus, the deformation mechanism used eliminates any anisotropy of the model structure with respect to a particular draw direction. With 30% tensile strain, the orientation of the carbonate group seems to reach a plateau while the orientation of the Bisphenol group continues to increase. This type of behavior is typical for a bimodal system. The geometric constraint on the large unit (or longer rod) drives them to align parallel to each other in the draw direction while the small unit (or shot rod) has more freedom to fit into the space. The change of properties upon deformation, therefore, can be expected to be mainly due to the alignment of these Bisphenol groups in the polymer.

3. Chain Configuration. The radius of gyration tensor (ellipsoid) characterizes the overall shape and orientation of a polymer chain. Upon deformation there

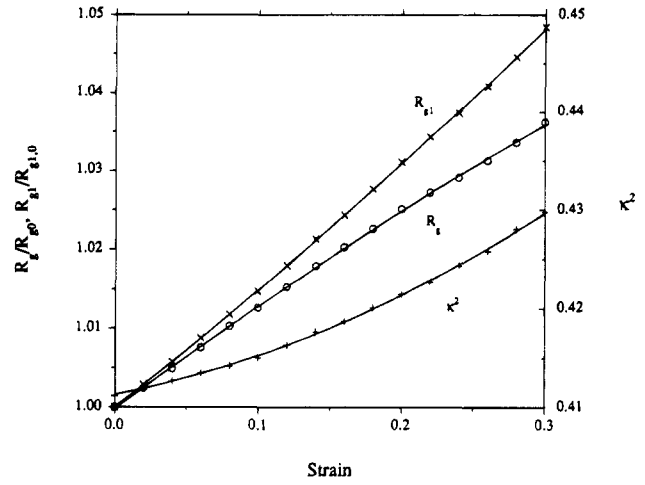

Figure 13. Changes of chain dimension and relative anisotropy as a function of strain.

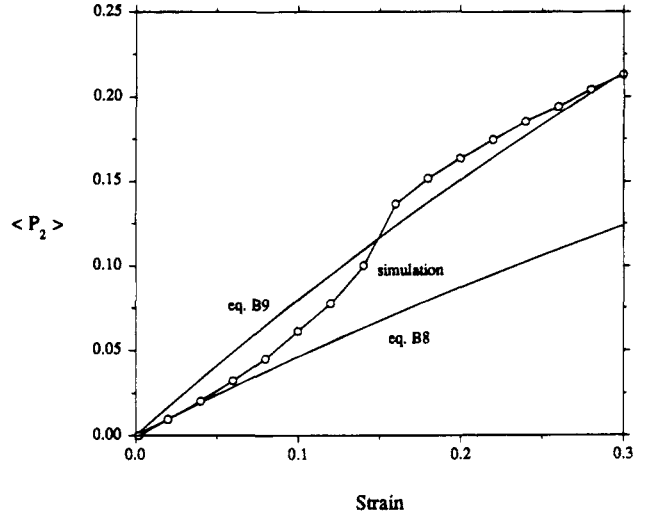

Figure 14. Orientation of the longest principal axis of the radius of gyration tensor of the model polymer during deformation.

will be two basic changes of the ellipsoid: it will rotate toward the draw direction while being elongated. The definition and calculation of the radius of gyration tensor as well as related variables can be found in ref 19. Here we use the radius of gyration (R_g) and the square root of the longest principal axis (R_{g1}) to characterize the elongation of the chain and use the orientation function $\langle P_2 \rangle$ of R_{g1} with respect to the draw direction to characterize the orientation of the chain. Figure 13 shows the relative elongation of R_g and R_{g1} as a function of strain (R_{g0} and $R_{g1,0}$ are the R_g and R_{g1} before deformation). Simulation data indicate that the R_{g1} is elongated more than the R_g. The relative larger deformation in R_{g1} leads to a larger anisotropy. This is shown in the same figure where the relative anisotropy invariant (κ^2)[19,20] as a function of strain is plotted. The orientation of the ellipsoids' major principal axis (R_{g1}) is shown in Figure 14 together with the calculated results from two relevant models (see Appendix B).

4. Expansion of Voids during Deformation. As the strain increases, the volume of the system increases too, consistent with the applied Poisson ratio. It is found that the volume change of the chain, estimated from the chain ellipsoid, is much less than the one of the system. At 30% strain the cell volume change is 11.1%, whereas the chain volume change is only 4.8%. This indicates that polymer segments like to stick together. However, upon deformation some parts of the chain will be separated to accommodate the overall volume increase in the system. Inevitably voids will emerge. Since the regions around those voids are the ones with the weakest cohesive interactions, they will grow as the strain increases. Eventually, they may even become defects capable of initiating structural failures.

Quantitative analysis of the voids, or free volume, in the atomistic model system has been studied recently.[21-24] The work by Misra and Mattice presented a very complete analysis of the free volume of polybutadienes.[24] Here, we adopt a similar approach to analyze the expansion of the voids in the model polycarbonate during tensile deformation. The basic procedure has four steps: (a) Generate a three-dimensional grid (increment = 0.4 Å) and impose it on the simulation cells; (b) assign the state of occupancy for each site in the grid (a site is occupied if it is within the van der Waals radii of the atoms); (c) find the connectivity between the vacant sites and define a void; (d) find the size of each void. The periodic boundary conditions are imposed in the calculation. This approach is capable of determining the exact size, shape, and location of each void in the system.

The calculated results show that the sum of all the voids in the system is about 19% of the total volume at zero strain. It is substantially larger than the fractional free volume of a typical glassy polymer (~2.5%)[25] or more recent experimental data by positron annihilation lifetime spectroscopy (PALS) (6.8–7.2%).[26] The difference can be explained by the size of the probe used.[21,24] In the calculation, an increase of the radius of the probe is equivalent to an increase of the van der Waals radius, which leads to a decrease in the free volume.[24] For example, increasing the van der Waals radii by 30% (using a probe with a radius of about 0.5–0.6 Å) reduces the void fraction to about 2.5%. About 80% of all the vacant sites are connected into a single large void. The rest are isolated empty sites (very small voids), scattered all over the system. These observations qualitatively agree with the earlier results on polybutadienes.[24] The largest sphere (~2–3 Å in radius) which can be put into the voids is only about $^1/_{20}$ of the volume of the biggest void. This is not surprising. Since the vacant sites are connected in a complex manner, the void shapes are mostly irregular rather than being spheroids. The complete analysis of the shape of the voids and connecting channels is interesting in itself.[22-24] In this paper, we only use the relative changes of three variables to characterize the development of voids: the total volume of the voids, the volume of the largest void, and the volume of the largest sphere that can be placed into these voids. Figure 15 shows the plots of these variables as a function of strain, together with the total volume changes. The growth of voids during the deformation process is obvious. Such observation agrees with the trend seen in experiments where the relative increase in the fractional free volume with strain measured by PALS is substantially larger than the fractional increase in bulk volume.[27] Experiments also indicate that the deformation scheme with the constant intrinsic Poisson ratio assumption is not valid at large strain since the volume of the bulk sample and the free volume actually may decrease as a function of strain.[26-28]

In theory the applied strain may extend far beyond the limits of this study. Such practice, however, causes at least two concerns: the convergence of structural optimization becomes much slower and the force field

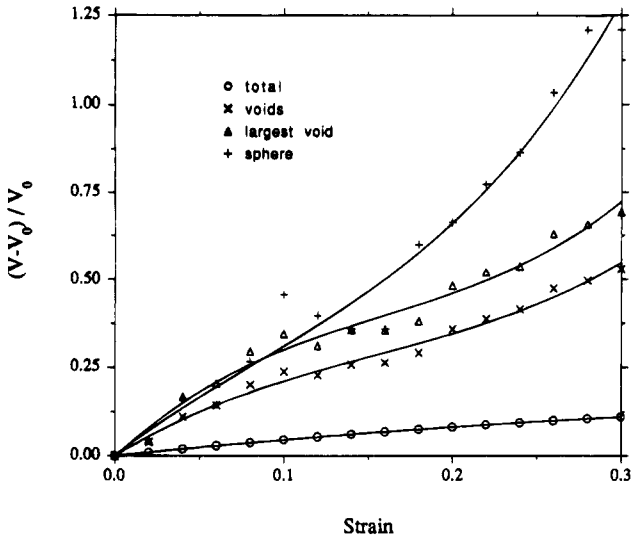

Figure 15. Relative changes of volumetric variables as a function of strain (see text for their definition).

may be inadequate. For example, when a material approaches failure, it is inevitable that the covalent bonds will be broken. However, no bonds will be broken in the simulation if only the harmonic potential is used as in most atomic simulations. Therefore, one needs to introduce a convenient form such as the Morse potential.[29] A more realistic deformation scheme needs to be developed as well, since the assumption of a constant intrinsic Poisson ratio certainly will fail. Without them the simulation may only generate highly distorted structures at very large strain but it will fail to reproduce experimental reality.

One interesting phenomenon that occurs after yielding for some ductile polymers is the formation of a neck; i.e., the cross section of one particular part of the sample is less than the rest. As deformation increases, the neck extends. In the modeling the bulk material was simplified by a unit cell and the periodic boundary conditions. Therefore the overall shape of the system always deforms uniformly across the simulation cell. No neck could be seen. However, the internal structural change associated with necking may still be observed in the simulation. Such change should occur much later due to the uniform deformation of the unit cell. The growth of a neck, known as cold drawing, normally occurs at a draw ratio larger than 2 (100% strain), which is beyond the strain limit of this study.

Conclusions

This study has shown that the source of yielding for amorphous materials under tension is the inflection on the Lennard-Jones potential (or similar potentials) if the van der Waals interactions are dominant in the deformation. No specific structural change is required near yielding. The voids develop during deformation since the volume change of the polymer chain lags behind the overall volume change of the system. Such a process has been clearly demonstrated through the analysis of the free volume of the system as a function of strain.

Acknowledgment. The author wishes to thank Dr. Tahir Cagin for many valuable discussions and suggestions in the course of this work as well as in the process of preparing this paper. Many helpful suggestions by Drs. Barry D. Olafson, K. A. Smith, and Wen Shi are also appreciated.

Appendix A. Apparent Poisson Ratio

Consider a cylinder with length L and radius r. When the cylinder is stretched in the L direction, the finite strains in the L and r directions (ϵ_L and ϵ_r) are

$$\epsilon_L = \frac{1}{2}\left(\frac{L^2}{L_0^2} - 1\right)$$

$$\epsilon_r = \frac{1}{2}\left(\frac{r^2}{r_0^2} - 1\right) \tag{A1}$$

where subscript 0 refers to the undeformed state. The corresponding infinitesimal strains can be defined as

$$\epsilon_L' = \frac{dL}{L} = d \ln L$$

$$\epsilon_r' = \frac{dr}{r} = d \ln r \tag{A2}$$

The (intrinsic) Poisson ratio can be defined as

$$\nu = -\frac{\epsilon_r'}{\epsilon_L'} \tag{A3}$$

and is assumed to be independent of strain. The apparent Poisson ratio at finite strain can be defined as

$$\nu_a = -\frac{\epsilon_r}{\epsilon_L} \tag{A4}$$

From eqs A2 and A4 one obtains $\nu\, d \ln L = -d \ln r$, $\nu \int_{L_0}^{L} d \ln L = -\int_{r_0}^{r} d \ln r$

$$\left(\frac{L}{L_0}\right)^{-\nu} = \frac{r}{r_0} \tag{A5}$$

and

$$\left(\frac{L^2}{L_0^2}\right)^{-\nu} - 1 = \frac{r^2}{r_0^2} - 1 \tag{A6}$$

Combining eqs A1, A4, and A6, the following relationship is reached:

$$\nu_a = \frac{1 - (2\epsilon_L + 1)^{-\nu}}{2\epsilon_L} \tag{A7}$$

Therefore the apparent Poisson ratio is a function of applied strain (ϵ_L) and the true Poisson ratio (v). At zero strain ν_a = v. The ν_a decreases as applied strain increases.

Appendix B. Orientation as a Function of Strain

Consider a system in which the vectors initially are randomly oriented. Before deformation the probability of finding vectors oriented at angle θ_0 ($0 \le \theta_0 \le \pi/2$) with the draw direction is

$$\varrho(\theta_0) = f(\theta_0)\, d\theta_0 \tag{B1}$$

where $f(\theta_0) = \sin \theta_0$ is the distribution function.[30] $\langle \cos^2 \theta_0 \rangle = 1/3$ and $\langle P_2 \rangle = 0$. After an affine deformation, all vectors initially oriented at θ_0 angle now orient at θ with respect to the draw direction. Thus, the probability of

finding θ is the same as initially finding θ_0[30]

$$f(\theta_0)\,d\theta_0 = f(\theta)\,d\theta \tag{B2}$$

Using $\tan\theta_0 = r_0/L_0$ and $\tan\theta = r/L$ and eq A1 (see Appendix A), one obtains

$$\tan^2\theta = C\tan^2\theta_0 \tag{B3}$$

where $C = (2\epsilon_r + 1)/(2\epsilon_L + 1)$ is a function of applied strain (ϵ_L) and the Poisson ratio (ν) and can be calculated from eqs A7 and A4. From eq B3 and trigonometric relationships, one can derive

$$\cos^2\theta_0 = \frac{C}{C + \tan^2\theta} \tag{B4}$$

$$\sin\theta_0 = \frac{\tan\theta}{(C + \tan^2\theta)^{1/2}} \tag{B5}$$

By differentiating both sides of eq B3, one has

$$d\theta_0 = \frac{\cos^2\theta_0}{C^{1/2}\cos^2\theta}\,d\theta \tag{B6}$$

Combining eqs B2, B4, B5, and B6, the new distribution function after deformation is obtained

$$f(\theta) = \frac{C^{1/2}\tan\theta}{(C + \tan^2\theta)^{3/2}\cos^2\theta} \tag{B7}$$

and the mean squared cosine theta, therefore, is

$$\langle\cos^2\theta\rangle = \int_0^{\pi/2}\cos^2\theta\, f(\theta)\,d\theta = \frac{1}{1-C} - \frac{C^{1/2}\sin^{-1}[(1-C)^{1/2}]}{(1-C)^{3/2}} \tag{B8}$$

Similarly, using eq B3 and trigonometric relationships, one finds that for an individual vector with initial orientation angle θ_0, the new angle θ after deformation is

$$\cos^2\theta = \frac{1}{1 + C\tan^2\theta_0} \tag{B9}$$

The P_2's with the $\langle\cos^2\theta\rangle$ from eqs B8 and B9 (θ_0 = 54.73) are shown in Figure 14.

References and Notes

(1) Mott, P. H.; Argon, A. S.; Suter, U. W. *Polym. Prepr. (Am. Chem. Soc., Div. Polym. Chem.)* **1989**, *30*, 34.
(2) Hutnik, M.; Argon, A. S.; Suter, U. W. *Macromolecules* **1993**, *26*, 1097.
(3) Mott, P. H.; Argon, A. S.; Suter, U. W. *Philos. Mag.* **1993**, *67*, 931.
(4) Brown, D.; Clarke, J. H. R. *Macromolecules* **1991**, *24*, 2075.
(5) Fan, C. F. *Polym. Mater. Sci. Eng.* **1993**, *69*, 24.
(6) Fan, C. F.; Cagin, T.; Chen, Z. M.; Smith, K. A. *Macromolecules* **1994**, *27*, 2383.
(7) Young, R. J. *Introduction to Polymers*; Chapman and Hall: London, 1981.
(8) Mayo, S. L.; Olafson, B. D.; Goddard, W. A. *J. Phys. Chem.* **1990**, *94*, 8897.
(9) Rahman, A. *Phys. Rev.* **1964**, *136*, A405.
(10) Parrinello, M.; Rahman, A. *J. Appl. Phys.* **1981**, *52*, 7182.
(11) Ray, J. R. *Comput. Phys. Rep.* **1988**, *8*, 109.
(12) Mark, J. E.; Erman, B. *Rubberlike Elasticity: A Molecular Primer* ; Wiley: New York, 1988.
(13) Mark, H. F.; Bikales, N. M.; Overberger, C. G.; Menges, G. *Encyclopedia of Polymer Science and Engineering*, 2nd ed.; Wiley: New York, 1988; Vol. 11 and references therein.
(14) Schramm, R. E.; Clark, A. F.; Reed, R. P. *A Compilation and Evaluation of Mechanical, Thermal, and Electrical Properties of Selected Polymers*; NBS Monograph 132, U.S. Government Printing Office: Washington, DC, 1973.
(15) Christiansen, A. W.; Baer, E.; Radcliffe, S. V. *Philos. Mag.* **1971**, *24*, 451.
(16) Nielsen, L. E. *Mechanical Properties of Polymers*; Chapman and Hall: London, 1961.
(17) Allen, M. P.; Tildesley, D. J. *Computer Simulation of Liquids*; Clarendon: Oxford, 1987.
(18) Donald, A. M.; Windle, A. H. *Liquid Crystalline Polymers*; Cambridge University Press: Cambridge, 1992.
(19) Theodorou, D. N.; Suter, U. W. *Macromolecules* **1985**, *18*, 1206.
(20) Woodward, L. A. *Introduction to the Theory of Molecular Vibrations and Vibrational Spectroscopy*; Clarendon: Oxford, 1972.
(21) Shah, V. M.; Stern, S. A.; Ludovice, P. J. *Macromolecules* **1989**, *12*, 4660.
(22) Rigby, D.; Roe, R. J. *Macromolecules* **1990**, *23*, 5312.
(23) Arizzi, S.; Mott, P. H.; Suter, U. W. *J. Polym. Sci., Polym. Phys. Ed.* **1992**, *30*, 415.
(24) Misra, S.; Mattice, W. L. *Macromolecules* **1993**, *26*, 7274.
(25) Aklonis, J. J.; MacKnight, W. J. *Introduction to Polymer Viscoelasticity*, 2nd ed.; Wiley: New York, 1983.
(26) Xie, L.; Gidley, D. W.; Hristov, H. A.; Yee, A. F. *J. Polym. Sci., Polym. Phys. Ed.* **1995**, *33*, 77.
(27) Ruan, M. Y.; Moaddel, H.; Jamieson, A. M.; Simha, R.; McGervey, J. D. *Macromolecules* **1992**, *25*, 2407.
(28) Powers, J. M.; Caddell, R. M. *Polym. Eng. Sci.* **1972**, *12*, 432.
(29) Welsh, W. J. In *Computational Modeling of Polymers;* Bicerano, J., Ed.; Marcel Dekker: New York, 1992; Chapter 2 and references therein.
(30) Kuhn, W.; Grün, F. *Kolloidzschr.* **1942**, *101*, 248.

MA9463066